HEAT AND MASS TRANSPORT CHARACTERISTICS IN VISCOUS SLIP FLOW OVER A CURVED SURFACE AND ENTROPY PRODUCTION

AMALA OLKHA[1], RAHUL CHOUDHARY[2*] and MUKESH KUMAR[3]

[1,2,3]Department of Mathematics, University of Rajasthan, Jaipur, 302004, Rajasthan, Jaipur

[*] Corresponding author; E-mail: rahulchoudhary535@gmail.com

This study deals with heat and mass transport in viscous slip flow over a curved, permeable sheet stretching linearly in a porous medium. Various factors influencing heat and mass transport, such as non-uniform heat generation/absorption, thermal radiation, chemical reaction, and viscous dissipation, are invoked in the study. Under appropriate similarity transformation relations, the governing nonlinear PDEs are turned into ODEs in non-dimensional form, and then tackled numerically utilizing MATLAB based bvp4c technique. The impacts of pertinent parameters are exhibited graphically on various relevant fields (velocity field, temperature field, concentration field) and discussed. Second law analysis is also presented in terms of entropy generation. Moreover, values of skin friction coefficient, Nusselt number, and Sherwood number are computed and presented in tabular form. For validity of the results obtained, the skin friction coefficient values are compared with previously published data and found to be in good agreement.

Key words*: Curved stretching sheet; Melting heat transfer; Slip; Porous medium; Non-uniform heat generation/absorption; Thermal radiation; Entropy generation*

1. Introduction

The heat and mass transport in viscous flow, under boundary layer assumptions, influenced by a heated stretching surface, manifest in several engineering processes such as extrusions, crystal growing, film blowing, fiber spinning and coating, hot rolling, etc. Crane **Error! Reference source not found.** presented pioneering work on laminar 2-D boundary layer viscous flow produced by a linearly stretching flat sheet. Crane's work, in various aspects, was further extended by many researchers including Cortell **Error! Reference source not found.**, Ibrahim and Shankar **Error! Reference source not found.**, Nayak et al. [4], and so forth.

In overhead investigations, it is commonly assumed that the fluid flow is produced by a flat stretching surface. But such a consideration may not be true in practical situations, for example, in thin films and extrusions. Consequently, Sajid et al. **Error! Reference source not found.** analyzed the viscous fluid flow influenced by a bended (curved) stretching sheet, and noticed that influence of curvature is noticeable within the boundary layer region. Abbas et al. **Error! Reference source not found.** extended this work and performed analysis of heat transport under prescribed surface temperature and heat flux conditions, in the presence of

magnetic field. Time-dependent flow due to a bended stretching/shrinking surface was explored by Rosca and Pop **Error! Reference source not found.**. Abbas et al. **Error! Reference source not found.** analysed MHD nanofluid flow produced by curved stretching sheet, considering the impacts of radiation and heat generation. Siddheshwar et al. **Error! Reference source not found.** discussed viscous nanofluid flow produced by a bended stretching sheet along with heat transport under prescribed heat flux and surface temperature conditions. Kumar et al. **Error! Reference source not found.** addressed electrically conducting Casson fluid flow over an exponentially stretching curved sheet accompanying magnetic field and radiation impacts. Sanni et al. **Error! Reference source not found.** examined viscous flow due to a quadratic curved stretching sheet and heat transport under influence of magnetic field.

In the preceding studies, the classical no-slip (full adherence) boundary condition was applied. However, there are fluids, such as emulsions and suspensions, that exhibit slip behaviour near the surfaces. The existence of slip is significant in several engineering processes, including micro heat exchangers and wire and fiber coating. Anderson **Error! Reference source not found.** studied slip effects in viscous flow influenced by a flat sheet stretching linearly. Subsequently, several researchers, including Ariel **Error! Reference source not found.**, Chauhan and Olkha **Error! Reference source not found.**, Ibrahim and Shankar **Error! Reference source not found.**, Olkha and Dadheech **Error! Reference source not found.**, have invoked slip boundary conditions in their studies on fluid flow produced by a stretching sheet.

In viscous dissipation process, kinetic energy (K.E) of the fluid transforms into heat energy which heats the fluid. It is an irreversible process and occurs because of viscosity. Its impact is similar to that of a heat source. Thus, altering fluid temperature and temperature gradient. This process has importance in aerodynamic heating, polymer processing, geological phenomena, denser space gases, and so forth. Partha et al. **Error! Reference source not found.** investigated impact of frictional heating in convection flow from an upright stretching surface in stagnant fluid and heat transport. In recent years, Alinejad and Samarbakhsh **Error! Reference source not found.**, Malik et al. **Error! Reference source not found.**, Srinivasacharya and Jagadeeshwar **Error! Reference source not found.**, Swain et al. **Error! Reference source not found.**, etc. invoked viscous dissipation impact in flow problems produced by stretching surfaces.

The study of heat-mass transport including chemical reaction over a stretching surface is important in several industrial and engineering processes like polymer production, food processing, and ceramics manufacturing. Due to chemical reaction, diffusing species may be produced or destroyed, and as a result, the quality and properties of the obtained product are affected. The order of the reaction significantly influences its impact. Postelnicu **Error! Reference source not found.** discussed influence of chemical reaction in heat and mass transport by natural convection from vertical surfaces in a porous medium. Impact of chemical reaction in two-dimensional flow of viscous fluid across a permeable stretching sheet under a magnetic field was investigated by Bhattacharyya and Layek **Error! Reference source not found.**. Malik et al. **Error! Reference source not found.** numerically investigated chemical reaction impact (homogeneous and heterogeneous) in Williamson flow outside a stretching

cylinder. Raju et al. **Error! Reference source not found.** presented heat-mass transport analysis in Casson fluid flow past a permeable stretching sheet, considering chemical reactions. Nagaraja and Gireesha **Error! Reference source not found.** examined non-Newtonian Casson fluid flow including heat-mass transport induced by a curved surface stretching in linear manner accompanied by magnetic field, chemical reaction, and space-dependent heat generation effects. Reddy et al. **Error! Reference source not found.** incorporated chemical reaction impact in viscous Newtonian flow over a permeable stretching surface including radiation and viscous dissipation effects.

The phenomenon of melting heat transport has several significant applications in engineering, particularly in thermal engineering, including latent heat storage, thermal insulation, welding processes, geothermal energy recovery, and magma solidification. Gorla et al. **Error! Reference source not found.** examined the melting heat transport in nanofluid flow past a permeable surface moving continuously. Melting heat transport in boundary layer flow of Powell-Eyring fluid in neighborhood of a stagnation point towards a stretching surface was explored by Hayat et al. **Error! Reference source not found.**. Hashim et al. **Error! Reference source not found.** considered melting effects in Carreau fluid flow influenced by a stretching cylinder. Gireesha et al. **Error! Reference source not found.** studied melting heat transport in dusty Casson flow due to a stretching sheet in the presence of magnetic field utilizing Cattaneo-Christov model. The results of study indicated that temperature field and thermal boundary thickness upsurge with Casson parameter. Olkha and Kumar **Error! Reference source not found.** incorporated melting effects in Casson fluid flow influenced by a curved stretching sheet.

It has been noticed that analysis based on second law of thermodynamics can serve to improve the design of thermal fluid flow and energy systems. Understanding the concept of irreversibility in thermodynamics and its minimization is important for engineers in optimizing thermal systems designs. The rate of entropy production is considered as a measure to quantify the significance of irreversibility in thermo-fluid flow systems. Entropy production concept and its optimization was introduced by Bejan **Error! Reference source not found.**. Later, Narla et al. **Error! Reference source not found.** assessed entropy generation in peristaltic flow in a curved channel. Baag et al. **Error! Reference source not found.** performed second law analysis in viscoelastic fluid flow through porous medium produced by a stretching sheet. In recent years, Narla et al. **Error! Reference source not found.**, Khan et al. **Error! Reference source not found.**, Olkha and Dadheech **Error! Reference source not found.**, and Mabood et al. **Error! Reference source not found.** have presented second law analysis in viscous Newtonian and non-Newtonian fluid flow due to a flat/curved stretching sheet. Ibrahim and Gizewu **Error! Reference source not found.** investigated entropy analysis in bioconvective viscous slip flow produced by a curved stretching sheet in the presence of micro-organisms. Olkha and Choudhary [43] examined entropy production in viscous slip flow in the existence of nanoparticles and micro-organisms influenced by an inclined sheet stretching exponentially.

In the overhead literature survey, it is found that a lot of work has been reported considering flat stretching sheet as flow geometry, but such a consideration may not be true in practical situations such as, in thin films and extrusions. It motivated us for the present work.

In this study, melting heat and mass transport in viscous slip flow influenced by a curved linearly stretching sheet are investigated. Various factors affecting fluid flow, thermal and mass transport (non-linear heat source, non-linear radiation, chemical reaction, porous medium, and viscous dissipation) are invoked in the study. The problem is solved numerically using MATLAB based bvp4c technique. The flow configuration and melting surface boundary condition are novel features of the investigation. Further, the inclusion of second law analysis in terms of entropy production also enriched novelty of the investigation. The study of flow problems with curved stretching surface as flow configuration finds applications in polymer industry, chemical and mechanical engineering, electronics, and oil industry, etc.

2. Problem Formulation

We consider boundary layer, time independent 2-D flow of chemically reactive, incompressible viscous fluid, through a porous medium produced by a curved permeable sheet stretching linearly (as shown in Figure 1). The sheet is curled along a circle having radius R. Since the surface is bended, therefore, a curvilinear coordinate system is assumed by taking, s the arc length and r, the radial direction. The cartesian and curvilinear coordinates are related by taking $x=\left(R+r\right)\cos(s/R)$ and $y=\left(R+r\right)\cos(s/R)$. We consider fluid flow to be influenced by stretching the sheet in arcual direction with velocity $u_w=as$, where $a>0$.

Under boundary layer assumptions, the governing equations with relevant characteristics, following Sajid et al. **Error! Reference source not found.**, are

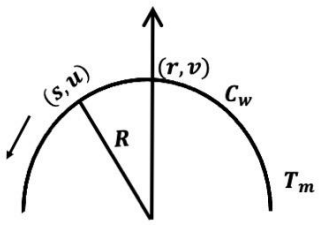

Figure 1 Geometry of the problem

$$\frac{\partial}{\partial r}\left\{\left(r+R\right)v\right\}+R\frac{\partial u}{\partial s}=0 \tag{1}$$

$$\rho\left(\frac{1}{r+R}u^2\right)=\frac{\partial p}{\partial r} \tag{2}$$

$$\rho\left(v\frac{\partial u}{\partial r}+\frac{Ru}{r+R}\frac{\partial u}{\partial s}+\frac{uv}{r+R}\right)=-\frac{R}{r+R}\frac{\partial p}{\partial s}+\mu\left[\frac{\partial^2 u}{\partial r^2}+\frac{1}{r+R}\frac{\partial u}{\partial r}-\frac{1}{\left(r+R\right)^2}u\right]-\frac{\mu}{K_p^*}u \tag{3}$$

$$\rho c_p\left(v\frac{\partial T}{\partial r}+\frac{Ru}{r+R}\frac{\partial T}{\partial s}\right)=k\left(\frac{\partial^2 T}{\partial r^2}+\frac{1}{r+R}\frac{\partial T}{\partial r}\right)+\mu\left(\frac{\partial u}{\partial r}-\frac{u}{r+R}\right)^2+q'''-\frac{1}{r+R}\frac{\partial}{\partial r}\left\{\left(r+R\right)q_r\right\} \tag{4}$$

$$v\frac{\partial C}{\partial r}+\frac{Ru}{r+R}\frac{\partial C}{\partial s}=D_B\left(\frac{\partial^2 T}{\partial r^2}+\frac{1}{r+R}\frac{\partial T}{\partial r}\right)-k_n\left(C-C_\infty\right)^n \tag{5}$$

where u and v represent the velocity components in arcual and radial direction respectively; R, radius of circle; p, the pressure; μ, the viscosity; ρ, the fluid density; K_p^*, the porous medium permeability; T, the fluid temperature; c_p, the specific heat (at constant pressure); κ, thermal conductivity of the fluid; q''', heat source/sink; q_r, radiative heat flux; C, fluid concentration; C_∞, fluid concentration far away from the surface; D_B, mass diffusivity; k_n, chemical reaction coefficient; and n, the order of reaction.

The adequate boundary conditions for the present problem are considered as

$$at\ r=0;\ u=u_w+l\left(\frac{\partial u}{\partial r}-\frac{u}{r+R}\right),\ v=-v_w+\frac{k}{\rho\left\{\left(T_m-T_0\right)c_s+\beta_m\right\}}\frac{\partial T}{\partial r},\ T=T_m,\ C=C_w$$

$$as\ r\to\infty;\ u\to 0,\ T\to T_\infty,\ C\to C_\infty \tag{6}$$

where, u_w, v_w, c_s, T_0, β_m, T_m, C_w, and T_∞, are stretching velocity, suction/injection velocity, solid surface heat capacity, solid surface temperature, latent heat, surface melting temperature, fluid concentration at the surface, and temperature far away from the surface (free stream temperature), respetively.

Following Abo-Eldahab and El Aziz **Error! Reference source not found.** heat generation or absorption $\left(q'''\right)$ depending on the space-temperature can be expressed as

$$q'''=\frac{\kappa}{\upsilon s}\left\{uA^*\left(T_m-T_\infty\right)+u_wB^*\left(T-T_\infty\right)\right\}, \tag{7}$$

where, $A^*, B^*>0$ represent internal heat generation while, $A^*, B^*<0$ represent internal heat absorption; u_w, the stretching velocity; and T_m, melting temperature.

Further it is assumed that the fluid is gray, non-scattering medium, and emitting-absorbing radiation. Unidirectional flux of thermal radiation is considered, which is transverse to the sheet.

Using Rosseland approximation, in optically thick fluid, the radiative heat transfer takes the form, following Pantokratoras and Fang **Error! Reference source not found.**, as follows:

$$q_r=-\left(\frac{4\sigma}{3k^*}\right)\frac{\partial T^4}{\partial r}=-\left(\frac{16\sigma}{3k^*}\right)T^3\frac{\partial T}{\partial r}, \tag{8}$$

where, k^* stands for the mean absorption coefficient for radiation and σ stands for Stefan-Boltzmann constant.

We introduce the following similarity transformation relations:

$$u=as\,f'(\eta),\eta=r\sqrt{\frac{a}{\upsilon}},v=-\frac{R}{r+R}\sqrt{a\upsilon}\,f(\eta),\quad p=\rho a^2s^2P(\eta),\ K=R\sqrt{\frac{a}{\upsilon}},$$

$$\theta(\eta)=\frac{T-T_\infty}{T_m-T_\infty},\ \phi(\eta)=\frac{C-C_\infty}{C_w-C_\infty}. \tag{9}$$

Using (9) into (1-5) and eliminating pressure p, we get

$$\left[f^{iv} + \frac{2f'''}{\eta+K} - \frac{f''}{(\eta+K)^2} + \frac{f'}{(\eta+K)^3} \right] - \frac{K}{\eta+K}\left[f'f'' - f\,f''' \right] - \frac{K}{(\eta+K)^2}\left[f'^2 - f\,f'' \right]$$
$$- \frac{K}{(\eta+K)^3} f\,f' - D\left(f'' + \frac{f'}{\eta+K} \right) = 0 \tag{10}$$

$$\theta'' + \frac{1}{\eta+K}\theta' + \frac{Pr\,K}{\eta+K} f\theta' + Br\left(f'' - \frac{f'}{\eta+K} \right)^2 + A^* f' + B^* \theta$$

$$+ R_d \left[\frac{1}{\eta+K}\left\{1+(\theta_w-1)\theta\right\}^3 \theta' + 3(\theta_w-1)\left\{1+(\theta_w-1)\theta\right\}^2 \theta'^2 + \left\{1+(\theta_w-1)\theta\right\}^3 \theta'' \right] = 0$$

(11)

$$\phi'' + \frac{1}{\eta+K}\phi' + \frac{Sc\,K}{\eta+K} f\phi' - Sc\,K_n\,\phi^n = 0 \tag{12}$$

and the transformed non-dimensional boundary conditions are:

$$at\ \eta = 0;\ f' = 1 + K_1\left(f'' - \frac{f'}{K} \right),\ f = S - \frac{Me}{Pr}\theta',\ \theta = 1,\ \phi = 1$$

$$as\ \eta \to \infty\ ;\ f' \to 0,\ \theta \to 0,\ \phi \to 0 \tag{13}$$

where, $K = R\sqrt{\frac{a}{\upsilon}}$, curvature parameter; $K_1 = l\sqrt{\frac{a}{\upsilon}}$, slip parameter; $D = \frac{\upsilon/a}{K_p^*}$, the porous medium parameter; $Pr = \frac{\mu c_p}{\kappa}$, Prandtl number; $Br = \frac{\mu u_w^2}{\kappa(T_m - T_\infty)}$, Brinkman number; $R_d = \frac{16\sigma T_\infty^3}{3\kappa k^*}$, radiation parameter; $Sc = \frac{\upsilon}{D_B}$, Schmidt number; $K_n = \frac{k_n (C_w - C_\infty)^{n-1}}{a}$, chemical reaction parameter; $S = \frac{v_w}{\sqrt{a\upsilon}}$, suction/injection parameter; $Me = \frac{(T_m - T_\infty)c_p}{\beta_m + c_s(T_m - T_0)}$, melting surface parameter; and $\theta_w = \frac{T_m}{T_\infty}$, temperature ratio parameter.

3. Skin friction coefficient, Nusselt number, and Sherwood number

The skin friction coefficient, Nusselt number, and Sherwood number are given by

$$C_f = \frac{\tau_w}{\rho u_w^2},\ Nu = \frac{sp_w}{\kappa(T_m - T_\infty)},\ Sh = \frac{sq_w}{D_B(C_w - C_\infty)}, \tag{14}$$

where, wall shearing stress (τ_w), surface heat flux (p_w), and surface mass flux (q_w), are given by

$$\left.\begin{aligned} \tau_w &= \mu\left(\frac{\partial u}{\partial r}-\frac{u}{r+R}\right)_{r=0}, \\ p_w &= \left(q_r-\kappa\frac{\partial T}{\partial r}\right)_{r=0}, \\ q_w &= -D_B\left(\frac{\partial C}{\partial r}\right)_{r=0}. \end{aligned}\right\} \tag{15}$$

Substituting values from (15) in (14) the expressions representing quantities of physical significance are obtained as:

$$\left.\begin{aligned} C_f\sqrt{\mathrm{Re}_s} &= \left[f''(0)-\frac{f'(0)}{K}\right], \\ Nu/\sqrt{\mathrm{Re}_s} &= -\left[1+R_d\left\{1+(\theta_w-1)\theta(0)\right\}^3\right]\theta'(0), \\ Sh/\sqrt{\mathrm{Re}_s} &= -\phi'(0). \end{aligned}\right\} \tag{16}$$

Here, $Re_x=\dfrac{as^2}{\upsilon}$ is local Reynolds number, C_f is skin friction coefficient, Nu is Nusselt number, and Sh is Sherwood number.

4. Entropy production

The entropy production, following Bejan **Error! Reference source not found.** and Arpaci **Error! Reference source not found.** and is given by

$$S'''_{gen}=\frac{\kappa}{T_\infty^2}\left(1+\frac{16\sigma T^3}{3\kappa k^*}\right)\left(\frac{\partial T}{\partial r}\right)^2+\frac{\mu}{T_\infty}\left[\left(\frac{\partial u}{\partial r}-\frac{u}{r+R}\right)^2+\frac{u^2}{K_p^*}\right]+\frac{D_B}{T_\infty}\left(\frac{\partial C}{\partial r}\frac{\partial T}{\partial r}\right)+\frac{D_B}{C_\infty}\left(\frac{\partial C}{\partial r}\right)^2 \tag{17}$$

where first term in RHS is entropy generation due to heat transport together with radiation effect, middle term is contribution due to viscous dissipation and porous medium, and last term is contribution due to mass transfer.

Using the transformation relations given by (9) in (17), entropy production in non-dimensional form obtained as

$$NS=\left[1+R_d\left\{1+(\theta_w-1)\theta\right\}^3\right]\theta'^2+\frac{\Gamma}{\Omega}\left[\left(f''-\frac{f'}{\eta+K}\right)^2+\frac{1}{K_p}f'^2\right]+\lambda_1\phi'\theta'+\lambda_2\phi'^2 \tag{18}$$

where, $NS=\dfrac{S'''_{gen}T_\infty^2(\upsilon/a)}{\kappa(T_m-T_\infty)^2}$, total entropy generation number; $\Gamma=\dfrac{\mu u_w^2}{\kappa(T_m-T_\infty)}$, Brinkman number; $\Omega=\dfrac{T_m-T_\infty}{T_\infty}$, non-dimensional temperature difference parameter; $\lambda_1=\dfrac{T_\infty D_B(C_w-C_\infty)}{\kappa(T_m-T_\infty)}$ and $\lambda_2=\dfrac{D_B T_\infty^{\,2}}{\kappa C_\infty}\left(\dfrac{C_w-C_\infty}{T_m-T_\infty}\right)^2$, the diffusion parameters.

5. Numerical Methodology

The nonlinear ordinary differential equations (10), (11) and (12), with the boundary conditions (13), are converted into a system of first-order ODEs and then numerically solved using the MATLAB software's built-in bvp4c program. Boundary value problems are handled by bvp4c using a collocation technique. The substitutes that were utilized are as follows:

$$\left(f, f', f'', f''', \theta, \theta', \phi, \phi'\right) = \left(y_1, y_2, y_3, y_4, y_5, y_6, y_7, y_8\right),$$

$$\frac{df'''}{d\eta} = \frac{K}{\eta+K}\left(y_2 y_3 - y_1 y_4\right) + \frac{K}{(\eta+K)^2}\left(y_2^2 - y_1 y_3\right) + \frac{K}{(\eta+K)^3} y_1 y_2 + D\left(y_3 + \frac{y_2}{\eta+K}\right) - \frac{2y_4}{\eta+K} + \frac{y_3}{(\eta+K)^2} - \frac{y_2}{(\eta+K)^3}, \tag{19}$$

$$\frac{d\theta'}{d\eta} = \frac{-1}{1+R_d\left(1+\left(\theta_w-1\right)y_5\right)^3}\left[\begin{array}{l} \frac{y_6}{\eta+K} + \frac{\Pr K}{\eta+K} y_1 y_6 + Br\left(y_3 - \frac{y_2}{\eta+K}\right)^2 + A^* y_2 + B^* y_5 \\ +R_d\left[\frac{1}{\eta+K}\left\{1+\left(\theta_w-1\right)y_5\right\}^3 y_6 + 3\left(\theta_w-1\right)\left\{1+\left(\theta_w-1\right)y_5\right\}^2 y_6^2\right] \end{array}\right], \tag{20}$$

$$\frac{d\phi'}{d\eta} = -\frac{2y_8}{\eta+K} - \frac{\mathrm{Sc}K}{\eta+K} y_1 y_8 + ScK_n y_7^n, \tag{21}$$

The following are the initial conditions:

$$\mathrm{y}_1(0) = \mathrm{S} - \frac{\mathrm{Me}}{\mathrm{Pr}}\mathrm{y}_6(0),\ \mathrm{y}_2(0) = 1 + \mathrm{K}_1\left(\mathrm{y}_3 - \frac{\mathrm{y}_2}{\mathrm{K}}\right),\ \mathrm{y}_3(0) = 0,\ \mathrm{y}_5(0) = 1,\ \mathrm{y}_7(0) = 1,$$

$$\mathrm{y}_4(0) = \alpha_1,\ \mathrm{y}_6(0) = \alpha_2,\ \mathrm{y}_8(0) = \alpha_3. \tag{22}$$

We use estimates to get the missing values of α_1, α_2, and α_3. Finally, equations 19 through 22 are added to Matlab's bvp4c function. The function handle @Odefun is included in the solver's syntax, sol = bvp4c(@Odefun, @Odebc, solinit, options), and is subsequently used to code equations (19)–(21). Next, the @Odebc function handle is coded with the boundary conditions (22). Choices is an optional integration parameter, while solinit is used to code the points of the initial mesh and the first estimation of the solution at the mesh points. To achieve the desired results, an educated estimate is first made at an initial mesh point, and the step size is then gradually reduced until the result is asymptotically met at the tolerance level of 10^{-6}.

6. Results and Discussion

The governing ODEs represented by (10-12) under boundary conditions represented by equation (13) are solved numerically by bvp4c technique on MATLAB with shooting method. For numerical calculations, we have chosen $Pr = 2$, $K = 5$, $D = 0.05$, $S = 0.05$, $Br = 0.07$, $R_d = 1.4$, $\theta_w = 0.6$, $A^* = 0.05$, $B^* = 0.05$, $Me = 0.3$, $K_n = 0.2$, $n = 2$, $Sc = 1.2$, $\Omega = 1.5$, $\lambda_1 = 0.2$, and $\lambda_1 = 0.3$, as fixed and altering these parameters one by one profiles of flow,

temperature distribution, concentration distribution, and entropy production are drawn for various values of the parameters occurred in the problem. For verification of current findings, skin friction coefficient values are compared with Abbas et al. **Error! Reference source not found.** as displayed in Table 1, and found in a good match.

Table 1 Comparison of skin friction coefficient values for various values of curvature parameter

Curvature parameter (K)	Abbas et al. **Error! Reference source not found.**	Present study (bvp4c)
5	1.15763	1.1648053478
10	1.07349	1.0765885386
20	1.03561	1.0372219279
30	1.02353	1.0247496824
40	1.01759	1.0186291068
50	1.01405	1.0149948589
100	1.00704	1.0077996579
200	1.00356	1.0042417998
1000	1.0008	1.0008667335

In Figures 2, 3, and 4 the function $f'(\eta)$, representing velocity distribution, is sketched for ascending values of melting surface parameter (Me), porous medium parameter (D), suction parameter (S), curvature parameter (K), and slip parameter (K_1). In these figures we observed, $f'(\eta)$ decreases with η and tends to zero at a distant position from the surface. As Figure 2 exhibits, the pace of the flow lessens by rising the melting parameter (Me) value. Physically, increase in Me value means increase in melting temperature which requires more transport of heat energy from fluid towards the surface, consequently energy level of the fluid particles decreases and hence fluid motion reduces. Thus, by rising melting parameter, flow field lessens and the corresponding boundary layer shrinks. Velocity field lessens with upsurge in porous medium parameter value (or decreasing permeability) also, since Darcy resistance which opposes the flow augments by increase in D value. Similar effect is noticed due to suction parameter (S), as expected. Figure 3 depicts the curvature parameter (bending of surface) impact on the velocity profile. It illustrates, fluid flow accelerates with rise in curvature parameter (K) value. As value of R increases the curvature reduces and in the limiting case the sheet becomes flat. Effect of velocity slip parameter (K_1) is displayed in Figure 4. From the figure, observed that velocity field reduces with rising slip also.

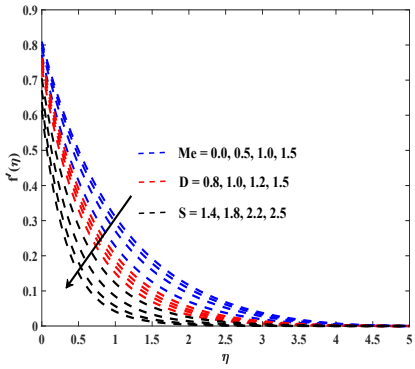

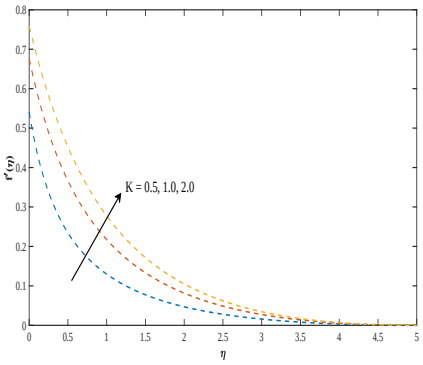

Fig. 2 Velocity Profile for Me, D, S. **Fig. 3 Velocity Profile for K.**

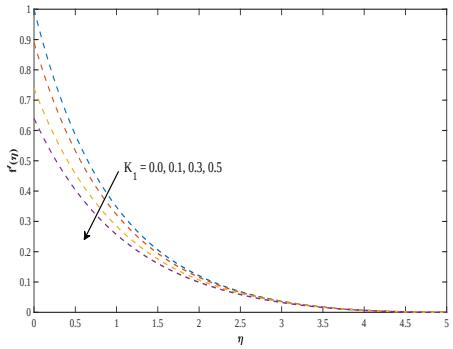

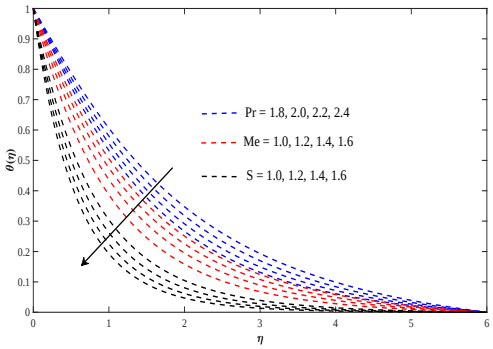

Fig. 4 Velocity Profile for K_1. **Fig. 5 Temperature Profile for $Pr, Me, and\ S$.**

Figure 5 exhibits variation in fluid's temperature for ascending values of relevant parameters. It depicts influence of Prandtl number (Pr), melting surface parameter (Me), and suction parameter (S) on fluid temperature. It depicts, fluid temperature lowers for upsurging value of Pr. Physically, an increase in the Prandtl number (Pr) value causes a reduction in thermal diffusivity, which results in a decrease in the fluid temperature field and consequently corresponding boundary layer thickness reduces. It is concluded from Figure 5 that the temperature distribution decreases with an increase in the melting parameter (Me) value. As the melting parameter (Me) rises, the flow rate decreases causing reduction in fluid temperature and thus the corresponding boundary layer shrinks. Similar effect is observed by increasing the suction parameter (S) at the stretching surface.

Figure 6 illustrates the alteration in temperature distribution, θ(η), for ascending values of the heat absorption parameters $\left(A^* < 0, B^* < 0\right)$ and porosity parameter (D). It is found that by increasing A^* (negative) and B^* (negative) values, the thermal boundary layer absorbs energy, causing a fall in the fluid's temperature. However, the effect of porous medium parameter D is noticed to increase the fluid temperature field.

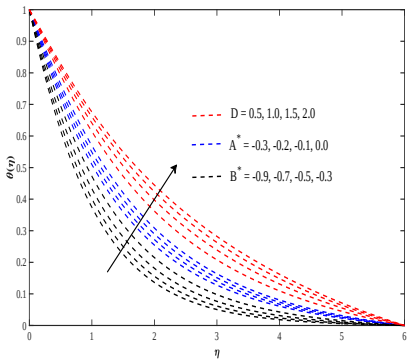

Fig. 6 Temperature Profile for D, A^*, B^*.

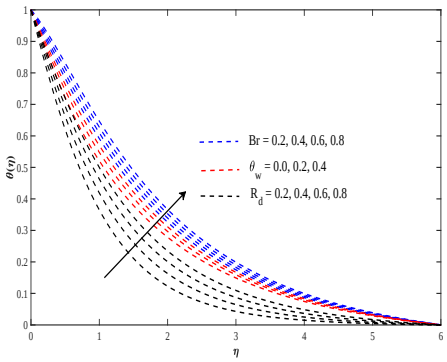

Fig. 7 Temperature Profile for Br, θ_w, R_d.

Figures 7 and 8 exhibit the impact of Brinkman number (Br), thermal radiation parameter (R_d), temperature ratio parameter (θ_w), and flow slip parameter (K_1) on temperature distribution. From Figure 7, an expansion in the fluid temperature field is observed wih an increase in the value of Br. Physically, the Brinkman number is a parameter that characterizes heat generation due to fluid friction (viscous dissipation) in the system. More heat produces for higher values of Brinkman number, leading to an augmentation in the temperature profile. The fluid temperature also rises with increasing radiation parameter (R_d) value. An increase in R_d implies a rise in heat transferred to the fluid due to radiation process, thereby enhancing the fluid temperature. The temperature field also expands with a rising value of the temperature ratio parameter, θ_w. A similar effect is observed due to velocity slip parameter, as depicted in Figure 8.

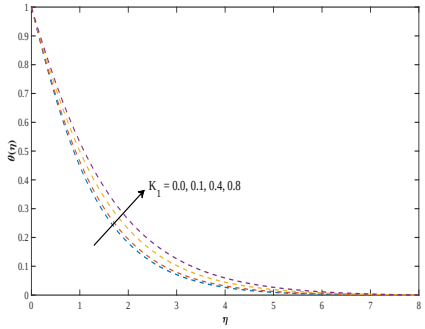

Fig. 8 Temperature Profile for K_1.

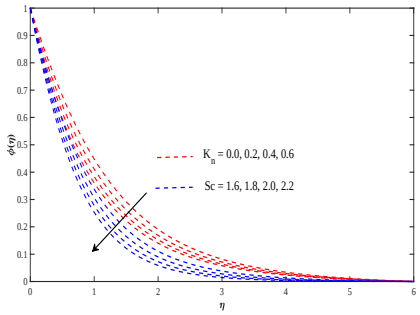

Fig. 9 Concentration Profile for K_n, Sc.

Figures 9 and 10 are drawn to exhibit the impacts of effective parameters on concentration distribution. In Figure 9 impacts of rising value of Schmidt number, Sc along with chemical reaction parameter, K_n are exhibited on concentration profile. From the figure it is concluded that concentration profile reduces for extending value of Sc. The reason behind is that mass diffusivity reduces with increasing value of Sc. Concentration profile also contracts with enhancement in K_n value, as shown in Figure 9. It happens due to species consumption

during the chemical reaction, therefore, reaction can be considered as destructive. Figure 10 depicts the impact of the order of the chemical reaction, n and velocity slip parameter, K_1. It is seen, concentration field expands by increasing the n value. The reason is that by increasing value of n concentration level increases and thus concentration profile improves. Similar influence due to slip is found, as the figure depicts.

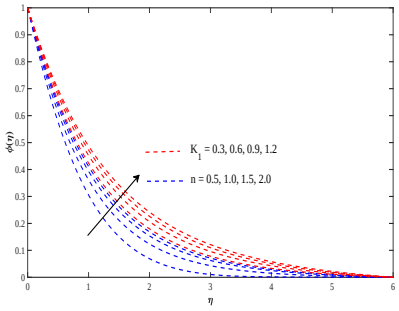

Fig. 10 Concentration Profile for K_1 and n.

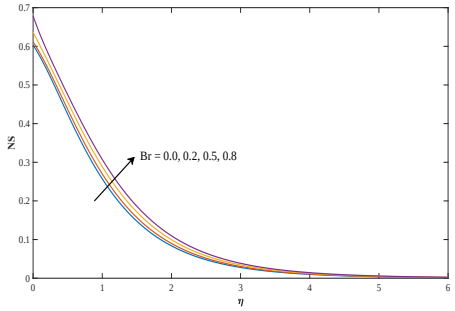

Fig 11 Entropy production for Br.

In Figures 11-16 variation in entropy production number NS is depicted for rising values of various pertinent parameters. These figures show higher entropy production in the region close to the surface. Figure 11 shows impact of Brinkman number Br on NS. It displays that NS increases with rising value of Br. Figure 12 exhibits effect of radiation parameter R_d on entropy production. It is concluded from this figure that with rising value of R_d the total entropy increases. Further, observed in Figure 13 that NS decreases with increasing value of temperature difference parameter (Ω). Similar effect is noticed for n, order of the reaction, as displayed in Figure 14 however, the reverse scenario is observed due to λ_1 and λ_2 as shown in Figures 15 and 16.

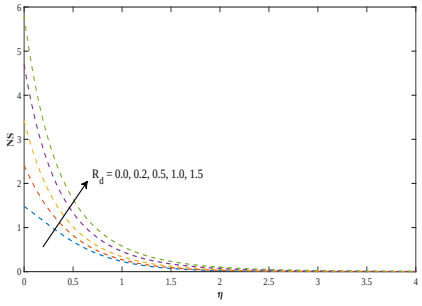

Fig. 12 Entropy production profile for R_d.

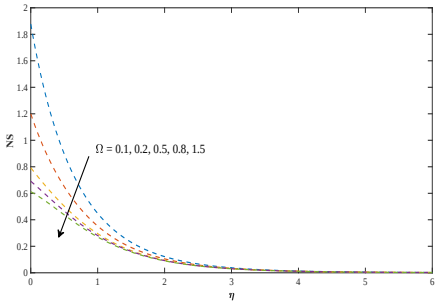

Fig 13 Entropy production profile for Ω.

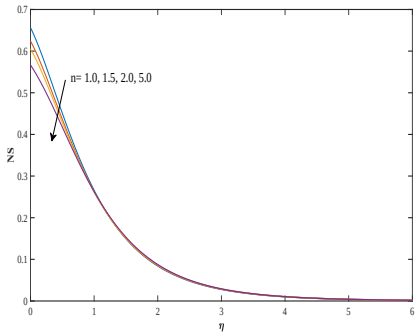

Fig. 14 Entropy production profile for n.

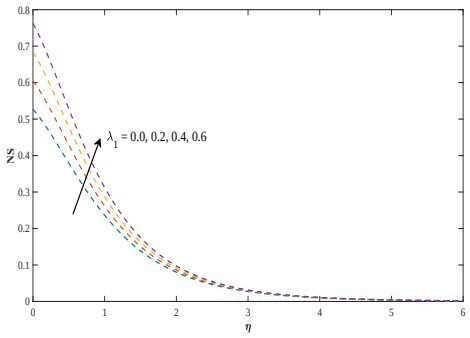

Fig. 15 Entropy production profile for λ_1.

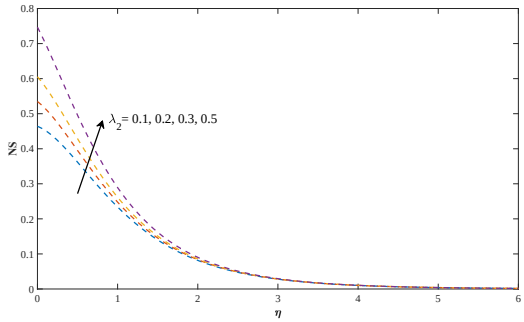

Fig. 16 Entropy production profile for λ_2.

Table 2 Skin friction coefficient values for various parameters

K	D	S	Me	Pr	K_1	$C_f(Re_s)^{1/2}$
0.5	0.5	1	0.3	2	0.2	-2.397076
1						-1.851155
2						-1.565721
	0.5					-2.397076
	1					-2.462033
	2					-2.555063
		1				-2.397076
		1.5				-2.431849
		2				-2.473483
			0.1			-2.389543

			0.3			-2.397076
			0.5			-2.406498
				1.8		-2.406711
				2		-2.397076
				2.2		-2.396808
					0.1	-3.161443
					0.2	-2.397076
					0.3	-1.931576

Table 3 Nusselt number values for various parameters

K	D	S	Me	Pr	Br	A^*	B^*	R_d	θ_w	K_1	$Nu/(Re_s)^{1/2}$
0.5	0.5	1	0.3	2	0.2	0.2	0.2	0.2	0.2	0.2	1.713813
1											2.277336
2											2.467626
	1										1.725861
	1.5										1.721052
	2										1.715580
		1									1.713813
		1.5									3.287907
		2									4.684358
			0.1								1.257151
			0.3								1.713813
			0.4								2.053771
				1.8							1.264358
				2							1.713813
				2.2							2.110811
					0.1						1.900679
					0.2						1.713813
					0.3						1.525234
						0.1					1.849546
						0.2					1.713813
						0.3					1.571674
							0.1				2.282843
							0.2				1.713813
							0.3				1.424017
								0.2			1.713813
								0.4			1.512189
								0.5			1.348854

									0.1		1.703246
									0.3		1.723132
									0.5		3.176346
										0.1	1.556473
										0.2	1.713813
										0.3	1.774973

Table 4 Sherwood number values for various parameters

K	D	S	Me	Pr	Br	R_d	Sc	K_n	n	K_1	$Sh/(Re_s)^{1/2}$
0.5	0.5	1	0.3	2	0.2	0.2	1.5	0.2	2	0.2	2.365763
1											2.361757
2											2.351844
	0.5										2.365763
	1										2.354839
	1.5										2.345702
		1									2.365763
		1.5									3.269704
		2									4.225304
			0.1								2.154863
			0.3								2.365763
			0.5								2.539591
				1.8							2.313478
				2							2.365763
				2.2							2.400089
					0.1						2.397028
					0.2						2.365763
					0.3						2.334422
						0.1					2.392726
						0.2					2.365763
						0.3					2.342887
							1				1.806313
							1.5				2.365763
							2				2.952018
								0.1			2.297527
								0.3			2.428456
								0.5			2.541408
									1		2.571629
									2		2.365763

									3		2.299133
										0.1	2.381935
										0.2	2.365763
										0.3	2.349695

7. Conclusions

In this study melting heat and mass transport in viscous slip flow over a curved stretching sheet are investigated. The sheet is permeable and fluid flow is considered in a porous medium. The impacts of non-linear thermal radiation, non-uniform heat absorption, viscous dissipation, and chemical reaction are incorporated. Second law analysis is performed in terms of entropy production. The problem is tackled numerically utilizing MATLAB based bvp4c method. The main findings of the investigation are as follows:

1. The pace of the flow decreases with increasing values of melting parameter (Me), porous medium parameter (D), and the suction parameter (S), while it increases with increasing value of curvature parameter (K).
2. The temperature profile shrinks with an increase in melting parameter while, influence of Brinkman number is observed to enhance it. It also enlarges with radiation process while, reverse scenario is observed due to heat absorption parameters.
3. The concentration profile expands with increasing order of the chemical reaction however, reaction coefficient and Schmidt number reduce it.
4. Maximum entropy production occurs in the region close to the surface.
5. The entropy generation profile magnifies with rising values of Brinkman number, thermal radiation, and diffusion parameters but opposite effect is observed due to order of the reaction.

Acknowledgment

Two of the authors (Mr. Rahul Choudhary and Mr. Mukesh Kumar) are grateful to the UGC-CSIR, India, for providing financial support in the form of Senior Research Fellowship.

Nomenclature

A^*, B^*	heat absorption parameter [$Wm^{-2}K^{-1}$]	Br	Brinkman number [-]
C	fluid concentration [kgm^{-3}]	c_p	specific heat [JKgK]
C_f	local skin friction number [-]	C_∞	fluid concentration far away from the surface [kgm^{-3}]
D	porous medium parameter [-]	D_B	mass diffusivity [m^2s^{-1}]
f	dimensionless velocity [-]	K	curvature parameter [m^{-1}]
K_n	chemical reaction parameter [-]	K_p^*	porous medium permeability [m^2]

Me	melting surface parameter [K]	n	order of reaction [-]
NS	total entropy generation number [-]	Nu	local Nusselt number [-]
p	pressure [Nm^{-2}]	Pr	Prandtl number [-]
q'''	heat source/sink [Wm^{-2}]	q_r	radiation heat flux [Wm^{-2}]
R	radius of circle [m]	R_d	radiation parameter [-]
Re_x	local Reynolds number [-]	S	suction/injection parameter [ms^{-1}]
Sc	Schmidt number [-]	Sh	local Sherwood number[-]
T	fluid temperature [K]	θ_w	temperature ratio parameter [-]
Greek symbols			
μ	viscosity [$kgm^{-1}s^{-1}$]	ρ	fluid density [kgm^{-3}]
σ	Stefan-Boltzmann constant [$Wm^{-2}k^{-4}$]	κ	thermal conductivity [$Wm^{-1}K^{-1}$]
k^*	mean absorption coefficient [m^{-1}]	θ	dimensionless temperature [-]
ϕ	dimensionless concentration [-]	η	similarity variable [-]
Ω	non-dimensional temperature difference parameter [-]		

References

[1] Crane, L.J, Flow past a stretching plate, *Zeitschrift für angewandte Mathematik und Physik ZAMP*, *21*(1970), pp. 645-647.

[2] Cortell, R., Flow and heat transfer of a fluid through a porous medium over a stretching surface with internal heat generation/absorption and suction/blowing, *Fluid Dynamics Research*, *37* (2005), 4, pp. 231-245.

[3] Ibrahim, W., Shanker, B., Unsteady boundary layer flow and heat transfer due to a stretching sheet by quasilinearization technique, *World Journal of Mechanics*, *1*(2011), 6, pp. 288-293.

[4] Nayak, M.K, et al., Heat and mass transfer effects on MHD viscoelastic fluid flow over a stretching sheet through porous medium in presence of chemical reaction, *Propulsion and Power Research*, *5*(2016), 1, pp. 70-80.

[5] Sajid, M., *et al.*, Stretching a curved surface in a viscous fluid, *Chinese Physics Letters*, *27*(2010), 2, pp. 024703.

[6] Abbas, Z., *et al.,* Heat transfer analysis for stretching flow over a curved surface with magnetic field, *Journal of Engineering Thermophysics*, *22*(2013), pp. 337-345.

[7] Roşca, N.C., Pop, I., Unsteady boundary layer flow over a permeable curved stretching/shrinking surface, *European Journal of Mechanics-B/Fluids*, *51(2015)*, pp. 61-67.

[8] Abbas, Z., *et al.,* Hydromagnetic slip flow of nanofluid over a curved stretching surface with heat generation and thermal radiation, *Journal of Molecular Liquids*, *215*(2016), pp. 756-762.

[9] Siddheshwar, P.G., *et al.*, Flow and heat transfer in a Newtonian nanoliquid due to a curved stretching sheet, *Zeitschrift für Naturforschung A*, *72*(2017), 9, pp. 833-842.

[10] Kumar, A., *et al.*, Effect of thermal radiation on MHD Casson fluid flow over an exponentially stretching curved sheet, *Journal of Thermal Analysis and Calorimetry*, *140*(2020), pp. 2377-2385.

[11] Sanni, K.M., *et al.*, Heat transfer analysis for non-linear boundary driven flow over a curved stretching sheet with a variable magnetic field, *Frontiers in Physics*, *8* (2020), pp. 113.

[12] Andersson, H.I., Slip flow past a stretching surface, *Acta Mechanica*, *158*(2002), pp. 121-125.

[13] Ariel, P.D., *et al.*, The flow of an elastico-viscous fluid past a stretching sheet with partial slip, *Acta Mechanica*, *187*(2006), pp. 29-35.

[14] Chauhan, D.S., Olkha, A., Slip flow and heat transfer of a second-grade fluid in a porous medium over a stretching sheet with power-law surface temperature or heat flux, *Chemical Engineering Communications*, *198*(2011), 9, pp. 1129-1145.

[15] Ibrahim, W., Shankar, B., MHD boundary layer flow and heat transfer of a nanofluid past a permeable stretching sheet with velocity, thermal and solutal slip boundary conditions, *Computers & Fluids*, *75*(2013), pp. 1-10.

[16] Olkha, A., Dadheech, A., Unsteady magnetohydrodynamics slip flow of Powell-Eyring fluid with microorganisms over an inclined permeable stretching sheet, *Journal of Nanofluids*, *10*(2021), 1, pp. 128-145.

[17] Partha, M.K., *et al.*, Effect of viscous dissipation on the mixed convection heat transfer from an exponentially stretching surface, *Heat and Mass transfer*, *41*(2005), pp. 360-366.

[18] Alinejad, J., Samarbakhsh, S., Viscous flow over nonlinearly stretching sheet with effects of viscous dissipation, *Journal of Applied Mathematics*, *2012*(2012), S107, pp. 1-10.

[19] Malik, M.Y., *et al.*, Effects of viscous dissipation on MHD boundary layer flow of Sisko fluid over a stretching cylinder, *AIP Advances*, *6*(2016), 3.

[20] Srinivasacharya, D., Jagadeeshwar, P., Effect of viscous dissipation and thermophoresis on the flow over an exponentially stretching sheet, *International Journal of Applied Mechanics and Engineering*, *24*(2019), 2, pp. 425-438.

[21] Swain, B.K., *et al.*, Viscous dissipation and Joule heating effect on MHD flow and heat transfer past a stretching sheet embedded in a porous medium, *Heliyon*, *6*(2020), 10.

[22] Postelnicu, A., Influence of chemical reaction on heat and mass transfer by natural convection from vertical surfaces in porous media considering Soret and Dufour effects, *Heat and Mass transfer*, *43*(2007), 6, pp. 595-602.

[23] Bhattacharyya, K., Layek, G.C., Chemically reactive solute distribution in MHD boundary layer flow over a permeable stretching sheet with suction or blowing, *Chemical Engineering Communications*, *197*(2010), 12, pp. 1527-1540.

[24] Malik, M.Y., *et al.*, Homogeneous-heterogeneous reactions in Williamson fluid model over a stretching cylinder by using Keller box method, *AIP Advances*, *5*(2015), 10.

[25] Raju, C.S.K., *et al.,* Heat and mass transfer in magnetohydrodynamic Casson fluid over an exponentially permeable stretching surface, *Engineering Science and Technology, an International Journal*, *19*(2016), 1, pp. 45-52.

[26] Nagaraja, B., Gireesha, B.J., Exponential space-dependent heat generation impact on MHD convective flow of Casson fluid over a curved stretching sheet with chemical reaction, *Journal of Thermal Analysis and Calorimetry*, *143*(2021), pp. 4071-4079.

[27] Reddy, N.N., *et al.,* Velocity slip, chemical reaction, and suction/injection effects on two-dimensional unsteady MHD mass transfer flow over a stretching surface in the presence of thermal radiation and viscous dissipation, *Heat Transfer*, *51*(2022), 2, pp. 1982-2002.

[28] Gorla, R.S.R., *et al.,* Melting heat transfer in a nanofluid flow past a permeable continuous moving surface, *Journal of Naval Architecture and Marine Engineering*, *8*(2011), 2, pp. 83-92.

[29] Hayat, T., *et al.,* Melting heat transfer in the stagnation point flow of Powell–Eyring fluid, *Journal of Thermophysics and Heat Transfer*, *27*(2013), 4, pp. 761-766.

[30] Hashim, et al., Characteristics of melting heat transfer during flow of Carreau fluid induced by a stretching cylinder, *The European Physical Journal E*, *40*(2017), pp. 1-9.

[31] Gireesha, B.J., *et al.,* MHD flow and melting heat transfer of dusty Casson fluid over a stretching sheet with Cattaneo–Christov heat flux model, *International Journal of Ambient Energy*, *43*(2022), 1, pp. 2931-2939.

[32] Olkha, A., Kumar, M., Heat transfer characteristics in non-Newtonian fluid flow due to a naturally permeable curved surface and chemical reaction, *Heat Transfer*, *52*(2023), 8, pp. 5431-5453.

[33] Bejan, A., A study of entropy generation in fundamental convective heat transfer, (1979).

[34] Bejan, A., Entropy generation minimization, Boca Raton F L CRC press, (1996).

[35] Narla, V.K., *et al.,* Second-law analysis of the peristaltic flow of an incompressible viscous fluid in a curved channel, *Journal of Engineering Physics and Thermophysics*, *89*(2016), pp. 441-448.

[36] Baag, S., *et al.,* Entropy generation analysis for viscoelastic MHD flow over a stretching sheet embedded in a porous medium, *Ain Shams Engineering Journal*, *8*(2017), 4, pp. 623-632.

[37] Narla, V.K., *et al.,* Entropy analysis of MHD fluid flow over a curved stretching sheet, *AIP Conference Proceedings*, *2246*(2020).

[38] Khan, M. J., *et al.,* Entropy generation analysis in MHD flow of viscous fluid by a curved stretching surface with cubic autocatalysis chemical reaction, *The European Physical Journal Plus*, *135*(2020), 2, pp. 1-17.

[39] Olkha, A., Dadheech, A., Second law analysis for radiative magnetohydrodynamics slip flow for two different non-Newtonian fluids with heat source, *Journal of Nanofluids*, *10*(2021a), 3, pp. 447-461.

[40] Olkha, A., Dadheech, A., Second law Analysis for Casson fluid flow over permeable surface embedded in porous medium, *Nonlinear Studies*, *28*(2021b), 4.

[41] Mabood, F., *et al.*, Entropy generation in the magnetohydrodynamic Jeffrey nanofluid flow over a stretching sheet with wide range of engineering application parameters, *International Journal of Applied and Computational Mathematics*, *8*(2022), 98.

[42] Ibrahim, W., Gizewu, T., Analysis of entropy generation of bio-convective on curved stretching surface with gyrotactic micro-organisms and third order slip flow, *International Journal of Thermofluids*, *17*(2022), pp. 100277.

[43] Olkha, A., Choudhary R., Investigation of melting heat transfer in viscous nanofluid flow including micro-organisms and entropy generation due to an inclined exponentially stretching sheet, *Journal of Nanofluids, 13*(2024), 2, pp. 446-463.

[44] Abo-Eldahab, E.M., El Aziz, M.A., Blowing/suction effect on hydromagnetic heat transfer by mixed convection from an inclined continuously stretching surface with internal heat generation/absorption, *International Journal of Thermal Sciences*, *43*(2004), 7, pp. 709-719.

[45] Pantokratoras, A., Fang, T., Blasius flow with non-linear Rosseland thermal radiation, *Meccanica*, *49*(2014), pp. 1539-1545.

[46] Arpaci, V.S., Radiative entropy production—lost heat into entropy, *International Journal of Heat and Mass Transfer*, *30*(1987), 10, pp. 2115-2123.

Submitted: 19.07.2024

Revised: 06.11.2024

Accepted: 08.112024.